Catalysis Letters 61 (1999) 15–25

Kinetic model of an oxygen-free methane conversion on a platinum catalyst

M. Wolf, O. Deutschmann, F. Behrendt and J. Warnatz

Interdisziplinäres Zentrum für Wissenschaftliches Rechnen (IWR), Universität Heidelberg, Im Neuenheimer Feld 368, D-69120 Heidelberg, Germany
E-mail: markus.wolf@iwr.uni-heidelberg.de

Received 1 March 1999; accepted 11 May 1999

In many metal-catalyzed conversion processes of hydrocarbons at atmospheric pressure a carbonaceous overlayer quickly builds up at the catalyst covering nearly the whole surface. However, the metal still remains catalytically active. Several models have been proposed over the years to explain the crucial role of the carbonaceous overlayer during the conversion of hydrocarbons. The model presented here contemplates adsorbate effects, which means that surface carbon modifies the dehydrogenation activity of Pt. A hydrocarbon reaction mechanism on platinum, including C_1 and C_2 species, is established. The mechanism is based on elementary reactions offering the opportunity of using the same mechanism for a wide range of applications. It is also applied to extended simulations of higher pressures and smaller flow velocities revealing increased C_2H_6 yields under these conditions.

Keywords: oxygen-free methane conversion, platinum, carbon layer, catalysis, hydrocarbon surface kinetics, modeling

1. Introduction

Methane, the major component of natural gas, is widely distributed at sites around the world. However, many of these sites are inaccessible by pipelines (stranded natural gas). Thus, transportation of the stranded gas to consumers requires low-temperature liquefaction (liquified natural gas, LNG) or local conversion to liquid hydrocarbons. The use of natural gas as a feedstock in chemical and pharmaceutical industry is an alternative to crude oil whose supplies might run out in the next century. Moreover, flaring gas which is a permanent companion of all oil fields could be used more efficiently. So far, it is usually burnt to avoid explosions. This is not only a waste of resources but also a growing problem in view of the greenhouse effect.

There are mainly three approaches to converting CH_4 into higher hydrocarbons: the direct oxidative conversion of methane (OCM), the Fischer–Tropsch process via syngas and the non-oxidative conversion of methane (NOCM).

Over the last decades, research has mainly focused on oxygen-containing processes, either indirect ones as in the Fischer–Tropsch processes or direct ones as in the oxidative conversion of methane (OCM). In the Fischer–Tropsch processes CH_4 is converted into hydrocarbons, via synthesis gas, which is subsequently hydrogenated, e.g., to methanol. At short contact times, the partial oxidation of methane on Rh-coated alumina foam monoliths leads to high conversion and syngas selectivity, both above 90% [1,2]. The application of even shorter contact times (using Pt as a catalyst), in the range of 500 μs, converts CH_4 directly into acetylene [3].

In the presence of oxygen, the direct CH_4 conversion (oxidative conversion of methane, OCM) to C_2H_6, C_2H_4 (one of the most important raw materials in industrial production cycles), C_3H_n, C_4H_n (all of them commonly abbreviated as C_{2+} hydrocarbons) is thermodynamically feasible (exothermic), whereas the oxygen-free or dehydrogenative conversion is endothermic (two-step polymerization). OCM has been investigated extensively (a survey is given by Baerns et al. [4]) and is still most frequently used due to its higher methane conversion and yields of C_{2+} [5]. The oxygen-free methane conversion on metal surfaces, however, has only been studied by a few groups [6–9]. The state of the art for this process was recently summarized by Guczi et al. [10].

A major disadvantage of the OCM is its low selectivity towards C_{2+}, because considerable amounts of CH_4 are consumed forming CO and CO_2. In contrast to OCM, the non-oxidative conversion of methane (NOCM) offers a high selectivity towards C_{2+} products, but produces only small C_{2+} yields due to a low CH_4 conversion [11]. The reason for focusing on oxygen-free methane conversion is therefore to maintain the high C_{2+} selectivity, while simultaneously enhancing the CH_4 conversion and the C_{2+} yield, respectively. The NOCM is a two-step process with the first step consisting of a pure methane flow and the second step of using pure hydrogen to remove the carbon layer and to set free the hydrocarbons formed during the first step [7,8].

The optimization of the NOCM necessitates a detailed knowledge of the occurring gas-phase and surface chemistry. In this work, we use a one-dimensional model of a stagnation-point flow on a catalytically active platinum catalyst in order to study the first step of the NOCM numerically. The model includes detailed gas-phase and surface kinetics combined with a multi-component transport model. Although several detailed mechanisms exist, each fitting well in a narrow range of reaction conditions,

e.g., catalytic combustion [12,13], partial oxidation [1,14], etc., the demand for mechanisms which consist of elementary reactions has grown substantially during this decade. A concerted effort [15] is made to establish a more universally valid surface mechanism including C_1 (methane), C_2 (ethane) and oxygen chemistry at the platinum surface. The kinetic model presented here is part of these efforts encompassing the oxygen-free surface chemistry.

Based on a comparison between the experimental results of Belgued et al. [8] with our simulations, we have developed a surface reaction model for the NOCM. The simulation agrees with experimentally measured temperature-dependent formation rates of C_2H_6 and of H_2, as well as with the carbon coverage on the catalyst. The model which is evaluated here is also applied to high-pressure (10 bar) simulations to examine conditions which might improve C_{2+} yields but have not yet been tested experimentally.

2. Methods

2.1. Modeling and experiment

The experimental results of Belgued et al. [8] have been used to evaluate our surface mechanism. The catalyst used in the experiment consisted of 6.3 wt% Pt on silica with Pt particle sizes ranging between 0.9 and 3.5 nm and 75% of the particles being smaller than 2 nm. The corresponding dispersion of Pt is 65%, i.e., 65% of the total amount of catalyst is available as surface atoms. The catalyst (Europt I) is placed in a continuous-flow fixed-bed reactor made of a U-shaped quartz tube (4 mm inner diameter) operated at atmospheric pressure.

In our flow model we use a one-dimensional stagnation-point flow directed towards a solid catalyst to study NOCM. The dependent variables (density, momentum, temperature and mass fraction of the individual gas-phase species) are functions of the time and the distance perpendicular to the surface. This set of governing equations is closed by the ideal gas law. We use the equation systems as stated by Warnatz et al. [16]. The properties of the catalyst surface itself are introduced in the simulation as boundary conditions for these governing equations. Thus, the solution of the gas-phase problem is linked to the surface properties and the surface reaction mechanism. The variation of a gas species' mass fraction at the surface, which is determined by diffusive and convective processes as well as by the formation or consumption of that species in process, is described in a time-dependent equation. Details of the boundary conditions can be found in Deutschmann et al. [12]. The code computes the species' mass fractions, temperature and velocity profiles in the gas phase, as well as fluxes at the gas–surface interface, the surface coverage and temperature as a function of time. The program accounts for a finite-rate gas-phase and surface chemical kinetics. A simplified multi-component molecular transport model is used. The discretization of the Navier–Stokes equations describing the gas-phase and the boundary conditions leads to a differential–algebraic equation system, which is solved by a semi-implicit method using the solver LIMEX [17].

In the temperature range of 300–700 K, as studied in the present work, first studies using a gas-phase reaction mechanism consisting of 55 reactions among 13 species revealed the insignificance of gas-phase reactions in that temperature range. A gas-phase reaction scheme was therefore not used in the simulations and the question of comparability of the 3D-experiment and the 1D-model was reduced to the influence of transport phenomena. Both the flow rate and the catalyst geometry determine product selectivity [18]. The flow rate dominates the thickness of the boundary layer and, hence, mass transport and residence time of species on the surface, respectively. A larger flow rate corresponds to a thinner boundary layer and, thus, considering the low sticking coefficients of CH_4 (see below), transport is fast in comparison to the CH_4 adsorption reactions. Belgued et al. [19] examined the effect of an increasing flow rate and found growing C_2 product selectivity for the two-step process. The highest flow rate used in their studies is 400 $\mathrm{cm^3\,min^{-1}}$; it represents an asymptotic limit. For the simulation, the experimental flow rate of 400 $\mathrm{cm^3\,min^{-1}}$ is transformed into a one-dimensional flow rate, dividing the experimental flow rate by πr^2, with r being the radius of the U-tube (2 mm). In order to compare the measured rates with the simulation, the former are first transformed into turnover frequencies and then multiplied by the platinum surface density of a (111) surface (2.49×10^{-9} $\mathrm{mol\,cm^{-2}}$). If comparisons are made between two reactors of different geometry, as it is the case between Belgued's experiment and our simulation, it is necessary that the process observed is not limited by transport but exclusively by surface kinetics. Due to the low CH_4 sticking coefficient on Pt, transport is much faster than surface kinetics under the conditions chosen in this work.

2.2. Kinetic model

The surface chemistry is modeled using a set of elementary reactions. The formation rate of species i, $\dot{s}_i$, is calculated by equation (1) with the rate coefficient k_{f_k} given in an extended Arrhenius form (equation (2)), which can account for a coverage dependence of the pre-exponential factor as well as of the activation energy (equation (3)) [20]. The formation rate of a species i, $\dot{s}_i$, is given by

$$\dot{s}_i = \sum_{k=1}^{K_\mathrm{s}} \nu_{ik} k_{f_k} \prod_{j=1}^{N_\mathrm{g}+N_\mathrm{s}} [X_j]^{\nu'_{jk}} \quad (i = 1, \ldots, N_\mathrm{g} + N_\mathrm{s}), \quad (1)$$

where K_s is the number of elementary surface reactions (including adsorption and desorption), ν_{ik} and ν'_{jk} are the appropriate stoichiometric coefficients, N_g and N_s are the number of gas species and adsorbed species. The concentration $[X_j]$ of an adsorbed species $(N_\mathrm{g} + 1, \ldots, N_\mathrm{g} + N_\mathrm{s})$ is given in $\mathrm{mol/cm^2}$ and equals the surface coverage (Θ_i) multiplied by the surface site density (Γ_i^τ).

The rate coefficient k_{f_k} is calculated by

$$k_{f_k} = A_k T^{\beta_k} \exp\left[\frac{-E_{a_k}}{RT}\right] f_k(\Theta_1, \ldots, \Theta_{N_s}), \qquad (2)$$

where A_k and E_{a_k} are the pre-exponential factor and the activation enthalpy of a reaction k. T^{β_k} allows for a more complex temperature dependence to be taken into account. The dependence of the reaction rate on the coverage of surface species i is taken into consideration by an additional function $f_k(\Theta_i)$,

$$f_k(\Theta_1, \ldots, \Theta_{N_s}) = \prod_{i=1}^{N_s} \Theta_i^{\mu_{i_k}} \exp\left[\frac{\varepsilon_{i_k}\Theta_i}{RT}\right], \qquad (3)$$

where μ_{i_k} describes the modified reaction order in respect to species i and ε_{i_k} the coverage-dependent activation enthalpy.

Alternatively, instead of pre-exponential factors, initial sticking coefficients may be used for the reaction input of adsorption processes. Then, the usual rate coefficients are given by

$$k_{f_k}^{\text{ads}} = \frac{S_i^0}{1 - S_i^0\theta_v/2} \frac{1}{\Gamma_i^\tau} \sqrt{\frac{RT}{2\pi M_i}} \exp\left[\frac{-E_{a_k}}{RT}\right], \qquad (4)$$

where S_i^0 is the initial sticking coefficient and Γ_i the surface site density to τ, the number of surface sites involved in the adsorption process. R represents the general gas constant, θ_v the coverage of free surface sites, T the absolute temperature in Kelvin, E_{a_k} the activation enthalpy of reaction k and M_i the molar mass of species i.

The surface mechanism consists of 14 surface species involved in 39 elementary surface reactions describing adsorption, desorption, recombination and C_2 isomerization. The surface mechanism is restricted to C_1H_x and C_2H_x species, since due to the introduction of C_3H_x species and even higher hydrocarbons an almost infinite number of isomerization reactions has to be taken into account. In the surface mechanism, forward and reverse reaction data can be given separately if there are deficiencies of thermodynamic data, which are given as polynomial coefficients [21,22]. Forming a reaction mechanism makes it necessary to know the reaction enthalpies ΔH of all surface reactions and, therefore, the surface standard enthalpies of formation ΔH_f^0 (298 K) of all species involved. The standard enthalpy of formation ΔH_f^0 (298 K) of the surface species j is calculated as the sum of the standard enthalpy of formation of species j in the gas phase and the heat of adsorption of species j at the surface. The heats of adsorption (adsorption enthalpies) for all C_1 and C_2 species are taken from Shustorovich [23]. These values are based on the bond-order conservation Morse potential (BOC-MP) method of Shustorovich et al. [24]. The necessity of generating a consistent data set on the one hand and the lack of data for several species on the other hand makes some adaptions inevitable. The principle of "additivity of bond properties" [25] was applied for those species whose heats of adsorption on Pt had to be guesstimated. In reactions where the activation enthalpies calculated by Shustorovich led to inconsistencies within the mechanism, adjustments were made (referred to in table 1). In the adjustment process, top priority was given to the heats of adsorption. For the temperature range 300–700 K, the standard enthalpies of formation ΔH_f^0 (298 K) are used in the simulation without a temperature correction. The lack of temperature correction is not expected to cause serious errors, because only the differences of the standard surface enthalpies of formation are used in the surface mechanism and the difference of heat capacities of all species taking part in the reaction, ΔC_{pi}, tends to be very small (compensation effect [25]).

2.3. Surface mechanism

In order to establish a mechanism, it is important to take into consideration as many experimental facts as possible. The following facts have to be considered in the case of the non-oxidative methane conversion (NOCM) on Pt:

Within minutes after starting the process and depending on temperature, the catalyst surface becomes covered with a near-monolayer of a carbonaceous overlayer at atmospheric pressure. However, catalytic activity can be maintained for thousands of hours. The role of the carbonaceous overlayer remains an open question. It has been classified by several groups [7,26,27] to consist of at least three different species (α, β, and γ), according to its composition C_xH_y or its property of being removable by hydrogen at different temperatures. The carbonaceous overlayer consists of mobile C_xH_y species with varying hydrogen content depending on temperature and time-on-stream (TOS, i.e., the time after starting to expose the catalyst to the flux of methane). Eventually, a hydrogen-poor graphitic structure is formed, blocking the metal surface and inhibiting catalysis. Different explanations concerning the role of the overlayer in catalysis have been discussed [27–29]. The model of Somorjai postulates that decreasing hydrogen content makes the carbonaceous layer more and more immobile and impedes the creation of metal islands, the only place where hydrocarbon conversion is assumed to take place. It further claims two physically existing modifications of the carbon layer, a two-dimensional one (in our model represented by C(s)) at temperatures below approximately 550 K and a three-dimensional one (in our model represented by C_2(s)) at temperatures above 550 K. The model discussed in the present paper assumes a carbonaceous overlayer consisting of two carbidic species, an atomic one C(s) [10,30] and a C_2(s) species symbolizing a polymer species which does not inhibit the platinum surface. A graphite modification C_{graphit}(s) which only blocks the surface has also been included in the mechanism. The C_2(s) is a species introduced to take into consideration the transformation from the two-dimensional modification to the three-dimensional one, thus making room for a continuous CH_4 adsorption, as described in more detail beneath. Yet the composition of the carbonaceous layer as well as its reactivity towards hydrocarbon conversion are still not completely understood.

Table 1
Surface reaction mechanism for the adsorption of methane on platinum.[a]

	Reaction	A	β	E_a	S_0
R1	$H_2 + PT(s) \rightarrow 2H(s)$		0.0	0.0	0.046[c]
R2	$CH_4 + 2PT(s) \rightarrow CH_3(s) + H(s)$		2.3	72.20	1.23×10^{-8}
R3	$CH_4 + C(s) \rightarrow CHCH_3(s)$[b]		0.5	0.0	1.99×10^{-10}
	$\theta_{CSUM(s)}$		0.0	47.50	
R4	$C_2H_6 + 2PT(s) \rightarrow C_2H_6(s)$		0.0	0.0	1.0
R5	$C_2H_4 + PT(s) \rightarrow C_2H_4(s)$		0.0	0.0	1.0
R6	$2H(s) \rightarrow H_2 + 2PT(s)$	3.70×10^{21}	0.0	60.00[c]	
	$\theta_{PT(s)}$		0.0	15.00	
R7	$CH_3(s) + H(s) \rightarrow CH_4 + 2PT(s)$	1.00×10^{21}	0.0	50.00[d]	
R8	$CHCH_3(s) \rightarrow CH_4 + C(s)$	1.00×10^{14}	0.0	2.50	
	$\theta_{CSUM(s)}$		0.0	47.50	
R9	$C_2H_6(s) \rightarrow 2PT(s) + C_2H_6$	1.00×10^{16}	0.0	20.90	
R10	$C_2H_4(s) \rightarrow PT(s) + C_2H_4$	1.00×10^{16}	0.0	50.20	
R11	$CH_3(s) + PT(s) \rightarrow CH_2(s) + H(s)$	1.26×10^{22}	0.0	70.30[d]	
R12	$CH_2(s) + H(s) \rightarrow CH_3(s) + PT(s)$	3.09×10^{22}	0.0	0.0[d]	
R13	$CH_2(s) + PT(s) \rightarrow CH(s) + H(s)$	7.31×10^{22}	0.0	58.90[d]	
	$\theta_{CSUM(s)}$		0.0	50.00	
R14	$CH(s) + H(s) \rightarrow CH_2(s) + PT(s)$	3.09×10^{22}	0.0	0.0[d]	
R15	$CH(s) + PT(s) \rightarrow C(s) + H(s)$	3.09×10^{22}	0.0	0.0[d]	
R16	$C(s) + H(s) \rightarrow CH(s) + PT(s)$	1.25×10^{22}	0.0	138.00[d]	
R17	$C_2H_4(s) \rightarrow CHCH_3(s)$[b]	1.00×10^{13}	0.0	83.30[d]	
R18	$CHCH_3(s) \rightarrow C_2H_4(s)$	1.00×10^{13}	0.0	75.30[d]	
R19	$C_2H_5(s) + H(s) \rightarrow C_2H_6(s)$	3.70×10^{21}	0.0	41.80	
R20	$C_2H_6(s) \rightarrow C_2H_5(s) + H(s)$	1.00×10^{13}	0.0	57.70[d]	
R21	$2CH_3(s) \rightarrow C_2H_6(s)$	1.00×10^{21}	0.0	0.0	
R22	$C_2H_6(s) \rightarrow 2CH_3(s)$	1.00×10^{13}	0.0	124.50[d]	
R23	$CH_2(s) + CH_3(s) \rightarrow C_2H_5(s) + PT(s)$	4.00×10^{22}	0.0	0.0	
R24	$C_2H_5(s) + PT(s) \rightarrow CH_2(s) + CH_3(s)$	4.00×10^{20}	0.0	128.90[d]	
R25	$C_2H_5(s) + PT(s) \rightarrow CHCH_3(s) + H(s)$[b]	4.00×10^{22}	0.0	54.40[d]	
R26	$CHCH_3(s) + H(s) \rightarrow C_2H_5(s) + PT(s)$	4.00×10^{22}	0.0	29.30	
R27	$C_2H_5(s) + 2PT(s) \rightarrow CH_2CH_2(s) + H(s)$[b]	1.37×10^{22}	0.0	16.70	
R28	$CH_2CH_2(s) + H(s) \rightarrow C_2H_5(s) + 2PT(s)$	1.37×10^{20}	0.0	28.90[d]	
R29	$CH_2CH_2(s) \rightarrow CHCH_3(s) + PT(s)$[b]	1.00×10^{13}	0.0	87.40[d]	
R30	$CHCH_3(s) + PT(s) \rightarrow CH_2CH_2(s)$[b]	1.37×10^{21}	0.0	50.20[d]	
R31	$CHCH_3(s) + PT(s) \rightarrow CCH_3(s) + H(s)$	1.37×10^{20}	0.0	99.10[e]	
R32	$CCH_3(s) + H(s) \rightarrow CHCH_3(s) + PT(s)$[b]	1.37×10^{22}	0.0	75.30[d]	
R33	$CCH_3(s) + PT(s) \rightarrow CH_3(s) + C(s)$	4.00×10^{21}	0.0	46.90[d]	
	$\theta_{CSUM(s)}$		0.0	50.00	
R34	$CH_3(s) + C(s) \rightarrow CCH_3(s) + PT(s)$	4.00×10^{21}	0.0	46.00[d]	
R35	$2C_2(s) \rightarrow C_{graphit}(s)$	1.00×10^{21}	0.0	240.00	
	$\theta_{C_2(s)}$		0.0	-60.00	
R36	$2C(s) \rightarrow C_2(s) + PT(s)$	1.00×10^{21}	0.0	180.00	
	$\theta_{C(s)}$		0.0	-50.00	
R37	$C_2(s) + PT(s) \rightarrow 2C(s)$	1.00×10^{21}	0.0	185.00	
	$\theta_{C(s)}$		0.0	-50.00	
R38	$C(s) + H_2 \rightarrow CH_2(s)$		0.0	29.70	4.00×10^{-2}
	$\theta_{CSUM(s)}$		0.0	4.60	
R39	$CH_2(s) \rightarrow C(s) + H_2$	7.69×10^{13}	0.0	25.10	
	$\theta_{CSUM(s)}$		0.0	50.60	

[a] Units: A (mol, cm, s), E_a (kJ/mol), S_0 (–), sticking coefficient. Pt(s) denotes bare surface sites with a density of 2.49×10^{-9} (mol/cm^2), corresponding to Pt(111), $\theta_{C(s)}$ and $\theta_{Pt(s)}$ and $\theta_{CSUM(s)}$ describe the dependence of the activation energy (ε_{i_k} according to equation (3)) on the C(s) coverage or the vacant surface area, respectively. $\theta_{CSUM(s)}$ is a dummy variable defined as the sum of $\theta_{C(s)}$ and $\theta_{C_2(s)}$ underlining the fact that both carbidic surface species do have the same impact on the dehydrogenation capability of Pt.

[b] The standard formation enthalpies in the gas phase of the species $CHCH_3(s)$ and $CH_2CH_2(s)$, and the adsorption enthalpy for $CH_2CH_2(s)$, have been calculated according to the "additivity of bond properties", as described in [25, p. 24].

[c] Taken from [12]; coverage dependence has been modified, as indicated in [28].

[d] The activation enthalpies taken from [23] have been adapted to form a consistent reaction scheme which gives priority to the calculated formation enthalpies of the species involved.

[e] Taken from [24].

Belgued et al. [8] studied the NOCM to C_2H_6 and H_2 at atmospheric pressure with a silica-supported platinum (Pt) catalyst (Europt I) at different temperatures and flow rates [19]. The temporal development of the rate of formation of C_2H_6 at constant methane mass flow varies significantly depending on the temperature. At temperatures above 540 K, the formation rate of C_2H_6 declines with TOS, as one would expect with steadily increasing carbon coverage and assuming a pure platinum-catalyzed conversion. However, measurements at 523 K show that there is a rate maximum appearing approximately after 1 min TOS.

The CH_4 chemisorption on Pt has been found to be the rate-determining step (RDS) with sticking coefficients of CH_4 varying between 10^{-4} and 10^{-12}. Molecular-beam experiments result in the higher range of sticking coefficient (10^{-4}–10^{-7}) [6], because, in this case, all molecules have a higher kinetic energy than that corresponding to a Maxwell distribution under normal adsorption conditions. The lower part of the range (10^{-10}–10^{-12}) is found in high-pressure experiments [31]. The reason for this wide variation of sticking coefficients is not only a result of the different experimental methods applied, but also a consequence of the electronic influence that adsorbates (such as oxygen O(s) or carbon C(s)) have on the metal surface.

While establishing a model which accounts for the above mentioned facts, one has to consider the fact that a catalytic process involves a sequence of different steps including reactant chemisorption, surface diffusion, chemical rearrangement and product desorption. If the rate-determining step (RDS) in this sequence is the reactant chemisorption, as in the case of CH_4 conversion, the E_F-LDOS (local density of states at the Fermi energy at the surface which is identical with the number of electrons at the Fermi level on surface sites) can be used as an indicator to show whether adsorbates promote or poison the surface. Adsorbates which enhance the E_F-LDOS or decrease the work function ϕ lead to a greater availability of electrons and, hence, to higher reactivity towards reactant chemisorption. Hydrogen on Pt [32] decreases the E_F-LDOS or increases ϕ, respectively. Carbidic carbon C(s) increases the work function ϕ of the platinum metal, while graphitic carbon decreases it [33,34]. The enhancement of the Pt work function ϕ by carbidic carbon C(s) is accompanied by a negatively polarized or charged C(s) at the surface which explains increasing lateral interaction. The amount of such lateral interaction depends on carbon coverage. Tontegode [33] reports an about 0.6 eV increase at the metal surface in the case of Ir. Ir is in many respects quite similar to Pt, e.g., electronegativity, ionization energy, atomic radius. We therefore assume a coverage-dependent additional activation enthalpy of 50 kJ/mol for all reactions increasing the carbon C(s) coverage (R8, R13, R33, R39) shown in table 1. As a consequence, the dehydrogenation activity of the Pt surface (R13, R39) is modified with TOS by an increasing carbon coverage [35].

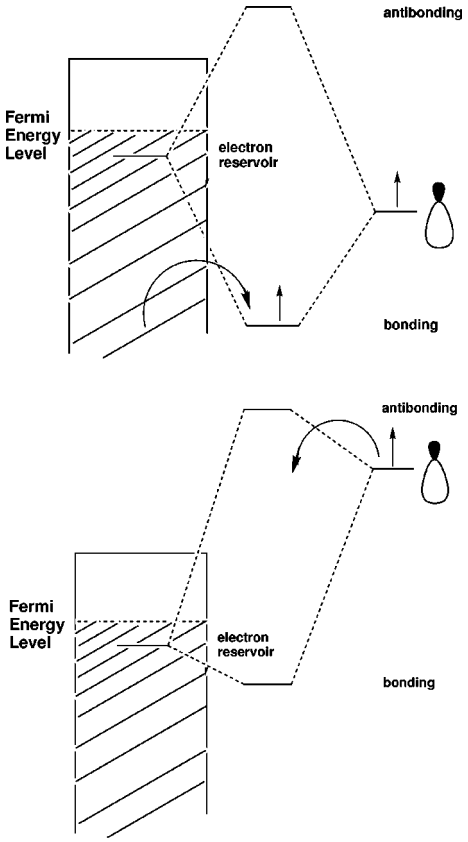

Figure 1. Interaction diagram between carbidic surface carbon and a metal surface due to Hoffmann's book [36, p. 114 ff]. This diagram shall stress the qualitative aspect of thinking over what kind of bonding to the surface might lead to the experimentally stated increase of the Pt work function by an increasing coverage of surface carbon [30,32].

Considering the role of the surface carbon within a surface mechanism it is necessary to think about the way carbon bonds to the metal surface. There are a lot of publications about how surface fragments can interact with metal bands or surface atoms, respectively. The latter perspective represents a more localized bonding view which is mainly described by Hoffmann [36] and Burdett [37].

Surface carbon can form σ and π bonds to the Pt surface. The σ bonds are formed with s and z^2 states of the metal, whereas the π bonds are formed by interacting with completely filled d-bands in the case of Pt. The polarization of the surface carbon depends on whether the singly occupied carbon frontier orbital lies above or beneath the Fermi energy level of the platinum metal, illustrated in figure 1.

If it lies beneath, the binding molecular orbital (MO) at first singly occupied by the carbon electron will be filled by an additional electron from the metal reservoir representing an electron transfer to the surface carbon [36]. This electron transfer leads to an increased work function ϕ, as indicated above [33,34].

If the carbon frontier orbital lies above the Fermi energy level of the metal, as it might be in supported metal catalysts where the support is very acidic or in zeolites, the electron transfer is vice versa leading to a decreased work function ϕ and a positively polarized surface carbon.

However, in any case a partial charge is imposed upon the surface carbon causing lateral interaction with an increasing coverage. In the surface model discussed in this paper we have focused on the effects lateral interactions have on the dehydrogenation capability of Pt and we have taken up model assumptions in regards to the carbon layer previously discussed in literature [27,28,39].

We did not consider possible modifications of the adsorption behaviour of Pt in respect to methane. This possibility cannot be excluded, because the interaction between singly occupied carbon orbitals and completely filled d-bands may lead to energetically enhanced antibonding molecular orbitals with radical- and carbon-like character. It is very probable that such radical-like states would make a heterolytical break of the C–H bond easier. Such a model in which surface carbon is directly involved in CH_4 chemisorption has been discussed in a former study [38].

The proposed surface mechanism is presented in table 1. There is one adsorption reaction (R3) where C(s) is directly involved in CH_4 chemisorption, and a very low initial sticking coefficient (lower than on Pt) is chosen for this sigmatrope insertion reaction. Its presence in the mechanism is due to microreversibility, since the reverse reaction R8 is supposed to be a necessary part of the mechanism. Only the CH_4 chemisorption on the uncovered Pt surface is considered to be important within this mechanism. No adsorbate effects, neither increasing nor decreasing the sticking probability of CH_4 on Pt, are considered in reaction R2. Instead, the adsorbate effect of carbidic carbon is taken into consideration by an increased activation enthalpy in reactions where carbidic carbon C(s) is produced, while the reaction enthalpy ΔH has been considered to be constant, as in R3/R8 and R38/R39.

The reactions in table 1, which are supposed to depend on the coverage of carbidic species, are formulated in dependence of a dummy variable $\theta_{\mathrm{CSUM(s)}} = \theta_{\mathrm{C(s)}} + \theta_{\mathrm{C_2(s)}}$ to account for the fact that both carbidic species have the same weight on modifying activation enthalpies. This was chosen because all carbidic species, C(s) as well as C_2(s), have the same impact on the Fermi level of the metal, as discussed above. In the case of graphite, there is an opposite effect [33,34], but it is not formed in the range of 300–700 K, as studied here. The pre-exponential factor for most reactions in table 1 was taken from the average frequency of the vibration mode of a chemical bond being in the range of 10^{13} in the case of a unimolecular reaction, and 10^{21} in the case of a bimolecular surface reaction. The latter value is calculated from the first one by dividing by the surface site density (concentration of Pt surface sites), which is 2.49×10^{-9} mol/cm^2. Values for pre-exponential factors which deviate from these standard values were found by including the reaction entropy of the reaction with the means of statistical thermodynamics. The reaction entropy influences the pre-exponential factor in terms of

$$A = A^0 \exp\left[\frac{\Delta S}{R}\right]. \qquad (5)$$

Including C_2(s) in this model (R36, R37, R35) is necessary in order to account for a carbon layer which exists in a two- and three-dimensional modification, depending on temperature. The C_2(s) formation makes room for further CH_4 adsorption and, therefore, catalytic activity is maintained.

For reproducing the experimental results, reactions R36 and R37 (2C(s) $\rightarrow$ C_2(s)) quickly have to establish a partial equilibrium and, hence, do not differ substantially in their activation enthalpies. The appearance of a three-dimensional carbon layer mainly above 550 K [27,28] calls for a minimum height of the activation enthalpy in R36/R37. Therefore, the standard formation enthalpy for C_2(s) is set at a value approximately twice as high as that of C(s).

Attempts to correlate C_2(s) with the thermodynamics of a known species failed without making more detailed assumptions, which are not justified by any experimental results. We therefore decided to keep the number of basic assumptions as low as possible.

3. Results and discussion

Models discussed in literature on hydrocarbon conversion on metal surfaces ascribe the main catalytic activity to the uncovered metal surface. Although it has been observed that the quickly forming carbon layer (under ambient pressure) has an impact on the process, most models restrict the role of the carbon layer to that of a hydrogen transmitter or placeholder [27,28,39]. A different model is discussed in [38] where the carbidic carbon is assumed to be an active part in the chemisorption of CH_4.

In comparison with experimental results and simulated ones, the surface reaction mechanism has to prove its reliability. As figures 2 and 3 clearly show, the measured and simulated rates of formation of C_2H_6 and H_2 compare qualitatively well. While at $T = 593$ K the experimental rate of formation of C_2H_6 decreases with time, as would be expected according to Somorjai [39] (at atmospheric pressure,

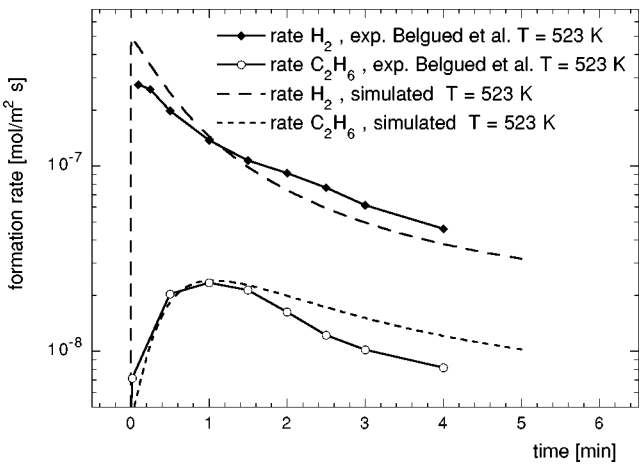

Figure 2. Comparison of experimental (lines with symbols, Belgued et al. [8]) and calculated (lines) rates of formation of C_2H_6 and H_2 (p = 1 bar, flow rate = 400 cm^3 min^{-1}, T = 523 K).

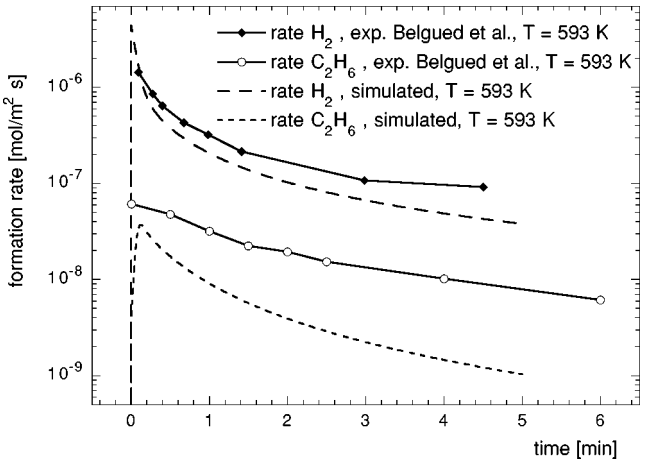

Figure 3. Comparison of experimental (lines with symbols, Belgued et al. [8]) and calculated (lines) rates of formation of C_2H_6 and H_2 (p = 1 bar, flow rate = 400 cm^3 min^{-1}, T = 593 K).

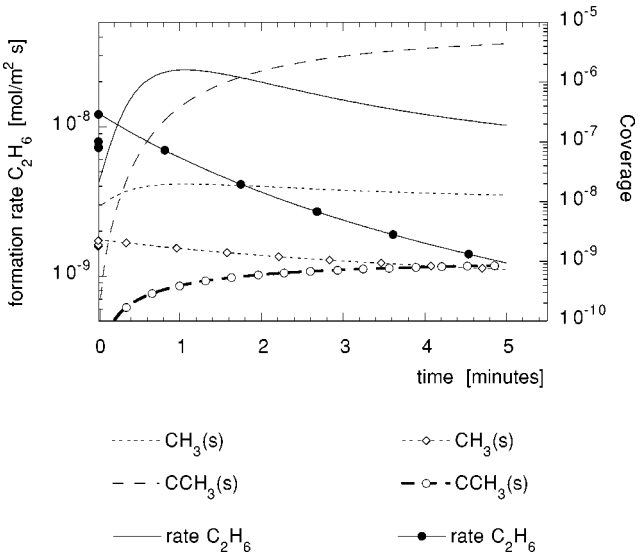

Figure 4. Temporal development of the C_2H_6 formation rate and of two important surface species, CH_3(s) and ethylidyne CCH_3(s), for a simulation in which the deposition of carbon C(s) modifies the dehydrogenation activity of the Pt surface (lines without symbols) and another simulation in which the carbon C(s) deposition just blocks the Pt surface (lines with symbols) (p = 1 bar, flow rate = 400 cm^3 min^{-1}, T = 523 K).

the catalyst surface is covered by a carbon layer within a few minutes, thus diminishing catalytic activity), the experimental points at T = 523 K exhibit a maximum. This maximum does not agree with a model which simply describes deactivation by carbon (blocking the active surface), as shown in figure 4. Belgued at al. [8] do not give any explanation for this maximum. The H_2 evolution is directly correlated with the formation of C_{2+}. The formation of hydrogen-deficient surface species is a prerequisite for the formation of carbon–carbon bonds. A comparison between figures 2 and 3 clearly shows that the ratio between the H_2 and the C_2H_6 formation rate is approximately ten, which corresponds well with the ratio measured. Hence, a carbon-coverage-dependent activation enthalpy for the dehydrogenation reactions, leading to carbidic carbon C(s) at the surface, is well suited to reproduce the formation rates of C_2H_6 and H_2 at the different temperatures shown in figures 2 and 3. It is assumed that there is also a maximum of the formation rate of C_2H_6 at T = 593 K which appears so early in TOS that is has not yet been experimentally resolved.

Good accordance between simulation and experiment can also be observed, if the simulated carbon coverage and the measured CH_x coverage are plotted as a function of temperature, as shown in figure 5. The difference in designation of carbon and CH_x is due to the different models of carbon layers established by different groups [7,26,28]. Our mechanism shows CH_3(s) accumulation only at low temperatures (200 K). Above T = 250 K, only C(s) and H(s) are present on the metal surface, which corresponds to a quick and complete decomposition of CH_3(s) at the surface, as observed by Zhou and White [40] and Solymosi [41]. The CH_3(s) decomposition leads to carbidic carbon C(s) which forms dipoles at the surface which increase the lateral interaction and, hence, increase the activation enthalpy for further carbon deposit. The sensitivity analysis in view of the formation of C_2H_6, figure 6, and the reaction flow analysis for the simulation at T = 523 K for

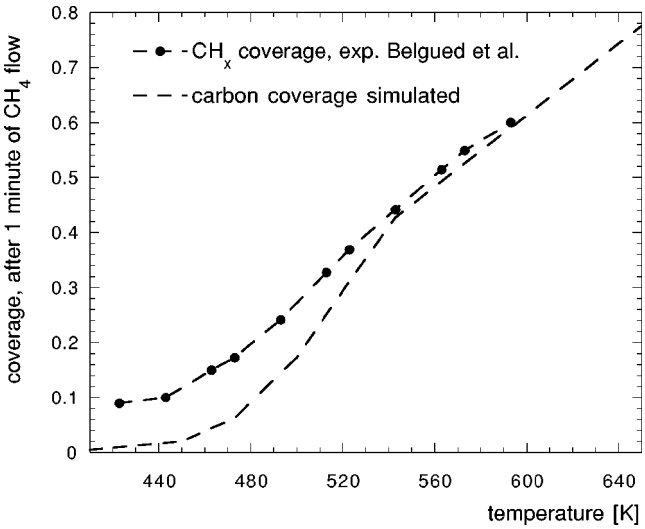

Figure 5. Comparison of experimental (line with symbols, Belgued et al. [8]) and calculated (dotted line) coverage of carbon or CH_x after 1 min of CH_4 flow at different temperatures (p = 1 bar, flow rate = 400 cm^3 min^{-1}).

different TOS reveal interesting details of the mechanism. At the beginning of the process, the recombination reaction of CH_3(s) (R21) forming C_2H_6 competes with R11 and R39, which decompose CH_3(s). At TOS = 1 s, 22.9% of the CH_3(s) species are decomposed to CH_2(s) (R12), from which 38% are further decomposed to C(s) and H_2 (R39). That competition changes drastically with TOS. While at TOS = 60 s, only 0.79% of the CH_3(s) species are decomposed to CH_2(s), approximately 93% of the CH_2(s) species are transformed back to CH_3(s) by hydrogenation, only 7% of CH_2(s) are still dehydrogenated to C(s) and H_2, due to

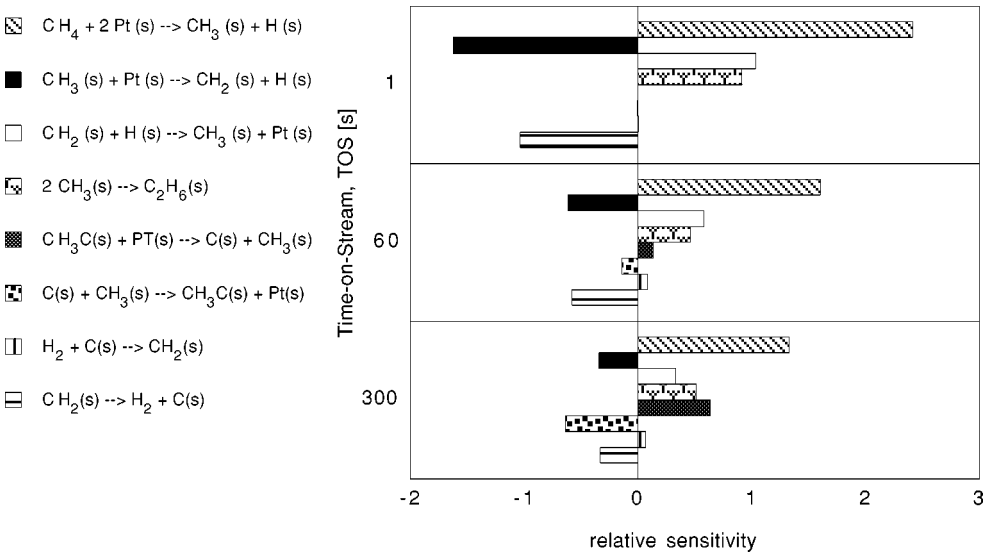

Figure 6. Temporal development of the relative sensitivities of some important reactions in respect to the formation of C_2H_6. All the reactions in this diagram are shown including their pre-exponential factors and activation enthalpy in table 1.

the then higher activation enthalpy of R39. At $T = 523$ K, a maximum of the formation rate of C_2H_6 appears, accompanied by a maximum of CH_3(s) species at the surface, see figure 4. Apart from recombination to C_2H_6, CH_3(s) reacts with C(s) to form an ethylidyne species CCH_3(s), another C–C bond forming reaction. Ethylidyne is a key species in the mechanism presented here. As flow analysis shows, a partial equilibrium between ethylidyne and its dissociation products, C(s) and CH_3(s) (R33, R34), is established very quickly. This provides the process with a small, but continuous amount of CH_3(s), which can recombine to ethane. The formation of C_2H_6 shows an increasing sensitivity with TOS with respect to the ethylidyne equilibrium, thus influencing the yield of C_2H_6. The ethylidyne equilibrium also becomes the main reaction channel for the formation and consumption of CH_3(s). After 1 s, approximately 76% of CH_3(s) species take part in reaction R34, whereas 100% of CCH_3(s) are transformed back. After 300 s TOS, approximately 99.4% of the CH_3(s) species are involved in this equilibrium (R33, R34). The relative sensitivity changes, just like the reaction channels do. Apart from CH_4 chemisorption, the CH_3(s) decomposition and, vice versa, the hydrogenation of CH_2(s) are the most sensitive reactions (R11, R12, R39) at the beginning, yet, as mentioned before, after 300 s TOS, the reactions R33 and R34 dominate the process.

Hence, at the beginning a reasonable part of the CH_3(s) species formed by CH_4 chemisorption is dehydrogenated to carbidic carbon C(s) which polymerizes with TOS to another carbidic species C_2(s) forming graphite at higher temperatures (R35). With increasing TOS, the accumulation of carbon at the surface, the dehydrogenation of CH_x(s) species, is inhibited by higher activation enthalpies due to lateral interaction of carbon C(s). Therefore, CH_3(s) dimerizes or reacts together with C(s) to ethylidyne CCH_3(s).

The integration of the rate of formation of C_2H_6 over TOS (in the results presented in this paper the process was finished after 5 min) represents a quantitative measure for the yield of C_2H_6 produced in the process. The plot of the integrated formation rates of C_2H_6 versus the reaction temperature shows a maximum of C_2H_6 yield at approximately 520–530 K (figure 7). This maximum coincides with the maximum of C(s) coverage, also shown in figure 7. This result agrees with experimental work by Zi-Feng et al. [11]. The coincidence between the maxima of C_2H_6 yield and C(s) coverage underlines the importance of carbidic carbon being present at the surface in order to produce high C_{2+} yields. We agree with Zi-Feng et al. that there are other species of the carbonaceous layer than C(s) which play an active role in the formation of C_{2+}. Moreover, the determination of these species makes it necessary to include higher hydrocarbon species, such as C_3 and C_4 as well as their isomerization reactions into the mechanism. Doing that requires more reliable experimental data about surface reactions.

In the mechanism discussed here, a small percentage of CCH_3(s) is hydrogenated to $CHCH_3$(s) which mainly decomposes to CH_4, whereas a minor part of $CHCH_3$(s) forms CH_2CH_2(s) and, successively, C_2H_5(s).

The mechanism presented here has been used in simulations (NOCM) under completely different conditions than those in experiments, e.g., at higher pressures than 1 bar and/or at smaller flow rates. The results revealed that there are conditions which lead to higher yields of C_2H_6. Possible explanations need to focus on the interaction between transport to and from the surface on the one hand and surface kinetics on the other hand. While the diffusion coefficient is reversely proportional to pressure, the use of small flow rates strengthens the pressure effect on transport leading to a thick boundary layer with small gradients. The transport of all species is slowed down. As a

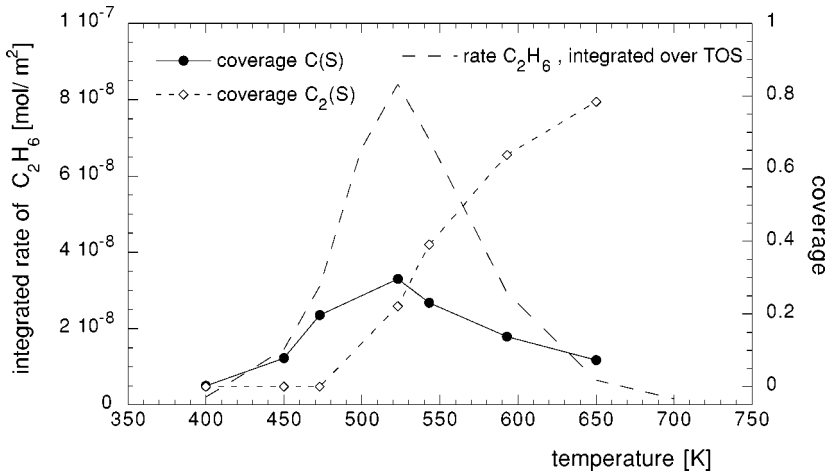

Figure 7. The formation rate of C_2H_6 integrated over the time-on-stream (TOS) (5 min) presents a quantitative measure of the C_2H_6 yield. It is obvious that the C_2H_6 yield is a function of temperature. The maximum yield of C_2H_6 can be found at approximately 520 K, coinciding with a maximum coverage of carbidic carbon C(s). The simulated results basically agree with experimental ones, as established by Zi-Feng et al. [11] ($p = 1$ bar, flow rate $= 400$ cm^3 s^{-1}, fuel $= 100\%$ CH_4).

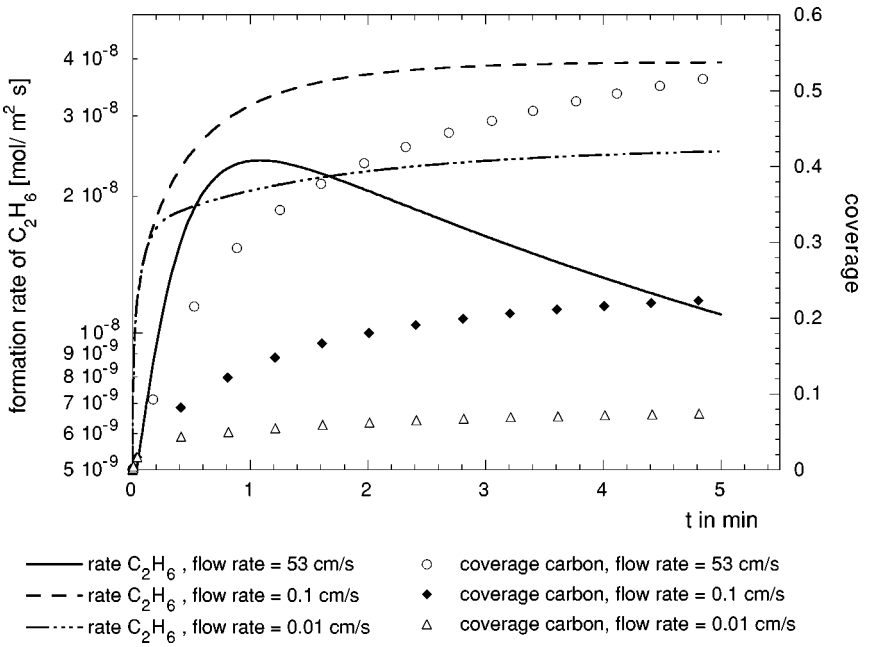

Figure 8. The effect of slowing down transportation by reducing the flow rate with regard to the formation of C_2H_6 and the carbon coverage at the platinum surface. Due to the computer model, flow rates are one-dimensional, as described in section 2.1 ($p = 1$ bar, $T = 523$ K, fuel $= 100\%$ CH_4).

result of such diminished transport, higher mole fractions of the products appear close to the surface, e.g., hydrogen, evolving from the Pt surface. An increased hydrogen concentration close to the surface means that the reaction $C(s) + H_2 \rightarrow CH_2(s)$ (R38) is substantially accelerated and, hence, the carbon deposit is decreased leading to higher and even time-independent formation rates of C_2H_6, as illustrated in figure 8. Figure 9 presents the correlation between the integrated formation rates of C_2H_6 at two different pressures, $p = 10$ and 1 bar, and various flow rates. It is obvious that there is still room for improvements. The ratio between the C_2H_6 yield at conditions where a maximum yield is expected and the C_2H_6 yield at conditions used in the experiment [5] (conditions described in figures 2 and 3) will be greater if the overall process time (in these simulations $= 5$ min) is increased. The reason for such an enhanced ratio with increased process time is that the formation rate of C_2H_6 at great flow rates drops significantly after 3–5 min TOS, while it remains at a higher level at smaller flow rates and/or higher pressures due to a smaller carbon deposit. It becomes clear from figure 8 that the process which runs at conditions achieving a maximum in the yield of C_2H_6 also shows a minimum in carbon coverage. With flow rates smaller than the ones shown in figure 8, the carbon deposit will even be smaller, but it does not lead to a greater yield of C_2H_6, as shown in figure 9.

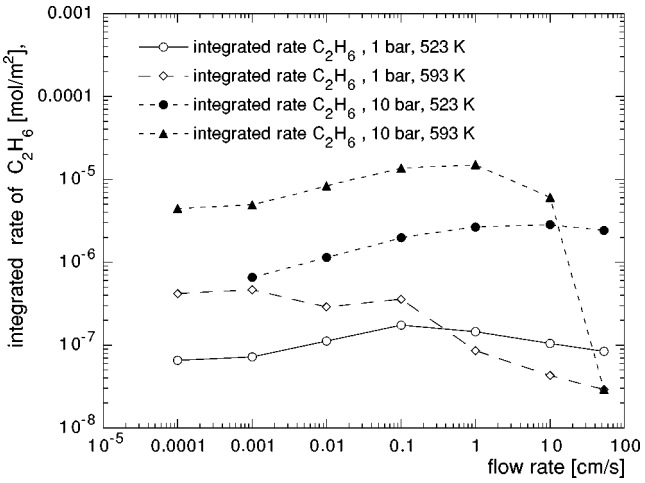

Figure 9. Integrated formation rates of C_2H_6, simulated at different pressures and temperatures, are plotted against the flow rate. Due to the computer model that was used (one-dimensional gas phase, see section 2.1), the flow rates are one-dimensional (overall time of the process $t = 5$ min).

This circumstance is caused by a limit in transport fixed by pressure and temperature, respectively. Beyond that limit, transport from and to the surface becomes too slow, thus limiting the overall process by overcompensating the positive effects of a slower transport, as mentioned above. It should be stressed again that, if transport becomes a limiting factor of the overall process or even so slow that it can be compared to the rate-determining surface reactions, then product selectivity is highly dependent on the geometry of the reactor [18,19]. A comparison of the results of our one-dimensional model with a three-dimensional reactor would therefore only make sense if the reactor's geometry would be the same for both. Hence, the results achieved for higher pressures and/or smaller flow rates have not yet been compared to experimental results measured in any reactor due to the lack of such high-pressure experiments. The only purpose of presenting these simulated results is to point out tendencies and possibilities for optimizing the NOCM process.

4. Conclusions

The advantage of the NOCM compared to the OCM is its higher C_{2+} selectivity; improving its poor yields could make it a valuable alternative. Acquiring detailed knowledge of its surface kinetics is a prerequisite for optimizing the CH_4 conversion of the NOCM. In the present work, we have made an attempt to achieve better insight into the process. Apart from reproducing the formation rates of C_2H_6 and H_2, as well as the carbon coverages, the present model gives a reasonable explanation why catalytic activity is maintained in the long run, although a major part of the Pt surface is covered by carbon. At the beginning of the process, dehydrogenation and hydrogenation of CH_x(s) species as well as CH_4 chemisorption are the most sensitive reactions, yet after 5 min TOS, the quickly established ethylidyne equilibrium (R33, R34) takes over this part, providing the process with a low but permanent concentration of CH_3(s) species. Detailed reproduction of experimental results was made possible by using a model of carbon which modifies the dehydrogenation activity of the Pt surface. The extent to which carbon modifies the dehydrogenation activity depends on its coverage. This is attained in the present model by an additional carbon-coverage-dependent activation enthalpy. Variations of process conditions as regards to pressure and/or flow rates showed that it is possible to enhance the yield of C_2H_6. So far, low C_2H_6 yields have been a major disadvantage of the oxygen-free CH_4 conversion compared to oxidative conversion of methane (OCM). There is an optimal flow rate for each pressure and temperature in view of the C_2H_6 yield. The increase in the C_2H_6 yield is due to low carbon coverages, the catalytic activity can therefore be maintained on the high starting level where no carbon deposits diminish the activity. The use of higher pressures makes it even possible to run the process at temperatures where at atmospheric pressure no catalytic activity would be visible due to the formation of graphite, which poisons the surface.

Acknowledgement

This work was supported by the Deutsche Forschungsgemeinschaft (DFG) within the Sonderforschungsbereich 359 "Reaktive Strömung, Diffusion und Transport".

References

[1] D.A. Hickman and L.D Schmidt, AIChE J. 39 (1993) 1164.
[2] A.S. Bodke and L.D. Schmidt, J. Catal. 179 (1998) 138.
[3] K.L. Hohn, P.M. Witt, M.B. Davis and L.D. Schmidt, Catal. Lett. 54 (1998) 113.
[4] M. Baerns, K. van der Wiele and J.R.H. Ross, Catal. Today 4 (1989) 471.
[5] J.A. Labinger, Quimica 48 (1993).
[6] M. Belgued, H. Amariglio, P. Pareja, A. Amariglio and J. Saint-Just, Catal. Today 13 (1992) 437.
[7] T. Koerts and R.A. van Santen, in: *New Frontiers in Catalysis*, Proc. 10th Int. Congress on Catalysis, eds. L. Guczi et al. (Elsevier, Amsterdam, 1993) p. 1065.
[8] M. Belgued, A. Amariglio, P. Pareja and H. Amariglio, J. Catal. 159 (1996) 441.
[9] F. Solymosi, A. Erdöhelyi and J. Cserenyi, Catal. Lett. 16 (1992) 399.
[10] L. Guczi, R.A. van Santen and K.V. Sarma, Catal. Rev. Sci. Eng. 38 (1996) 249.
[11] Y. Zi-Feng, X. Jin-Zhen, S. Shi-Kong and W. Hong-Li, J. Nat. Gas Chem. 5 (1996) 261.
[12] O. Deutschmann, R. Schmidt, F. Behrendt and J. Warnatz, in: *Twenty-Sixth Symposium (International) on Combustion* (The Combustion Institute, Pitsburgh, 1996) p. 1747.
[13] P.A. Bui, D.G. Vlachos and P.R. Westmoreland, Surf. Sci. 385 (1997) L1029.
[14] G. Veser, J. Frauhammer and L.D. Schmidt, in: *AIChE Meeting*, Los Angeles, 16–21 November 1997, paper 266d.
[15] Communications between D.K. Zerkle (Los Alamos National Laboratories), L.D. Schmidt et al. (University of Minnesota), and O. Deutschmann et al. (IWR, University of Heidelberg).

[16] J. Warnatz, M.D. Allendorf, R.J. Kee and M.E. Coltrin, Combust. Flame 96 (1994) 393.
[17] P. Deuflhard, E. Hairer and J. Zugck, Numer. Math. 51 (1987) 501.
[18] D.A. Hickman and L.D. Schmidt, J. Catal. 136 (1992) 300.
[19] M. Belgued, A. Amariglio, P. Pareja and H. Amariglio, J. Catal. 159 (1996) 449.
[20] K. Christmann, *Introduction to Surface Physical Chemistry*, Topics in Physical Chemistry (Springer, New York, 1991) p. 69.
[21] A. Burcat, in: *Combustion Chemistry*, ed. W.C. Gardiner (Springer, New York, 1984).
[22] R.J. Kee and J.A. Miller, in: *Complex Chemical Reaction Systems: Mathematical Modelling and Simulation*, eds. J. Warnatz and W. Jger (Springer, Heidelberg, 1987).
[23] E. Shustorovich, *Metal Surface Reaction Energetics* (VCH, Weinheim, 1991) pp. 191–223.
[24] E. Shustorovich and A.T. Bell, Surf. Sci. 205 (1988) 492.
[25] S.W. Benson, in: *Thermochemical Kinetics*, 2nd Ed. (Wiley–Interscience, New York, 1976) p. 22.
[26] H.P. Bonzel and H.J. Krebs, Surf. Sci. 91 (1980) 499.
[27] G.A. Somorjai, *Introduction to Surface Chemistry* (Wiley–Interscience, New York, 1994) p. 505.
[28] S.M. Davis, F. Zaera and G.A. Somorjai, J. Catal. 77 (1982) 439.
[29] S.J. Thomson and G. Webb, J. Chem. Soc. Chem. Commun. (1976) 526.
[30] T.M. Duncan, P. Winslow and A.T. Bell, Chem. Phys. Lett. 102 (1983) 163.
[31] F. Zaera, Chem. Rev. 95 (1995) 2651.
[32] Y.Y. Tong, A.J. Renouprez, G.A. Martin and J.J. van der Klink, in: *11th Int. Congress on Catalysis – 40th Anniversary*, Vol. 101 B, eds. J.W. Hightower, W.N. Delgass, E. Iglesia and A.T. Bell (Elsevier, Amsterdam, 1996) pp. 901–910.
[33] A.Ya. Tontegode, Prog. Surf. Sci. 38 (1991) 201.
[34] X.Q.D. Li, T. Radojicic and R. Vanselow, Surf. Sci. Lett. 225 (1990) L29.
[35] R. Schlögl, in: *Handbook of Heterogenous Catalysis*, Vol. 1, eds. G. Ertl, H. Knözinger and J. Weitkamp (Wiley–VCH, Weinheim, 1997) pp. 152–153.
[36] R. Hoffmann, in: *Solids and Surfaces: A Chemist's View of Bonding in Extended Structures* (Wiley–VCH, Weinheim, 1988) pp. 76 ff and 114 ff.
[37] K. Burdett, in: *Molecular Shapes* (Wiley–Interscience, New York, 1980).
[38] M. Wolf, O. Deutschmann, F. Behrendt and J. Warnatz, in: *Natural Gas Conversion V*, Stud. Surf. Sci. Catal., Vol. 119, eds. A. Parmaliana, D. Sanfilippo, F. Frusteri, A. Vaccari and F. Arena (Elsevier, Amsterdam, 1998) p. 271.
[39] G.A. Somorjai, in: *Chemistry in Two Dimensions: Surfaces* (Cornell University Press, Ithaca, NY, 1981) p. 483.
[40] X.L. Zhou and J.M. White, Chem. Phys. Lett. 142 (1987) 376.
[41] F. Solymosi, Catal. Today 28 (1996) 193.